High Temp. Mater. Proc., Vol. **30** (2011), pp. 181–191 DOI 10.1515/HTMP.2011.027

Corrosion of Aluminized and Uncoated 9–12 % Cr Boiler Steels in Simulated Biomass and Waste Combustion Conditions

Jarkko Metsäjoki,[1,*] **Elina Huttunen-Saarivirta**[1] **and T. Lepistö**[1]

[1] Department of Materials Science, Tampere University of Technology, Tampere, Finland

Abstract. Coatings are seen a promising way to improve the corrosion resistance of relatively cheap power plant steels to enable higher steam temperatures than currently in use. In this research, 9–12 % Cr steels P91 and HCM12A are coated with aluminium diffusion coating by a slurry method and exposed for 336 hours at 833 K and 883 K to atmospheres containing varying amounts of O_2, H_2O, HCl and SO_2. Corrosion behaviour of the coated steels is compared to that of those steels in an uncoated condition. Characterization is performed by weighing, SEM + EDS and XRD. The results show that corrosion resistance of P91 and HCM12A is significantly improved by the aluminium diffusion coating at high temperatures in atmospheres containing HCl and SO_2. The corrosion rate of the aluminized specimens slightly increases with increase in test temperature but remains virtually the same irrespective of the composition of the atmosphere. On the other hand, the corrosion rate of the uncoated specimens is dependent on both the atmosphere and the temperature. The steels undergo active oxidation that results in formation of non-protective, thick and layered scales in HCl containing atmospheres. SO_2 addition slightly decreases the corrosion rate although it is anyway higher than that in SO_2 containing atmosphere without HCl.

Keywords. Corrosion, slurry coating, P91, HCM12A, aluminizing, active oxidation.

PACS®(2010). 81.05.Bx, 81.65.Kn.

1 Introduction

Biomass combustion is an attractive choice for reduction of CO_2 emissions, because the CO_2 released in combustion is bound in the new growth of biomass i.e. biomass combustion is considered CO_2 neutral. In turn, the combustion of waste generally solves two simultaneous problems: the waste is disposed and heat and energy are produced in the same process. However, in these combustion processes, elevated temperature corrosion prevents raising the operating temperature to the level of conventional coal combusting plants. Both, biomass and waste include a wide variety of fuels and, thus, a wide variety of chemical compounds that affects composition of flue gases and deposits [1]. Sulphur content of most biofuels and combustable waste is relatively low when compared to coal, but the amount of chlorine can be very high. [2–4] Due to the high chlorine and low sulphur content, corrosion problems arise in boiler components such as superheater tubes. The main cause for severe corrosion has been referred to *active oxidation*, a cyclic process in which chlorine forms from HCl or other gaseous chlorides, penetrates into the scale and forms volatile metal chlorides at the metal-scale interface. Subsequently, the formed chlorides travel to the scale surface and leave the scale or oxidize at a higher partial pressure of oxygen in the scale, thus forming a thick and porous, unprotective, scale. The chlorine is released in the oxidation, and it returns to the metal-scale interface to react again. [5, 6] Because of the corrosion problems caused by *active oxidation*, steam temperature has to be kept relatively low; this reduces the electrical efficiency of the power plant. [7]

Coatings may provide a way to improve corrosion resistance of power plant materials. Aluminium diffusion coatings have been found [8–13] to perform well in water vapour containing atmospheres at high temperatures. Recent studies [14, 15] have shown that aluminium diffusion coatings significantly improve the corrosion resistance of several alloys also in HCl containing atmospheres, where the uncoated materials undergo severe corrosion by active oxidation [5, 6, 16–18]. These coatings can be easily applied to large components at the manufacturing site of the components [19]. This is a prerequisite for being used in power plant components.

This paper compares the corrosion behaviour of aluminized 9–12 % Cr power plant steels to that of these steels in an uncoated state. The aim is to apply coatings to improve corrosion resistance of relatively cheap power plant steels so that these materials can be employed at temperatures higher than currently used and thus to improve the electrical efficiency of a power plant. In this paper, infor-

Corresponding author: Jarkko Metsäjoki, Department of Materials Science, Tampere University of Technology, P.O. Box 589, FI-33101 Tampere, Finland; E-mail: jarkko.metsajoki@tut.fi.

Received: November 8, 2010. Accepted: November 26, 2010.

Alloy	Fe	Cr	Mn	Mo	Si	Ni	V	W	Cu
P91	88.2	9.2	0.50	0.90	0.40	0.38	0.22	< 0.005	
HCM12A	83.5	12.5	0.54	0.36	0.25	0.34	0.21	1.9	0.85
Alloy	**C**	**Nb**	**N**	**Ti**	**P**	**S**	**Al**	**Co**	**B**
P91	0.089	0.062	0.0489	0.006	0.013	< 0.001	0.010	0.008	
HCM12A	0.071	0.045	0.0569		< 0.01	< 0.001	0.012		< 0.005

Table 1. Chemical compositions (in mass %) of the steels.

Experiment	T [K]	N_2	H_2O [%]	O_2 [%]	HCl [ppmv]	SO_2 [ppmv]
1	833	bal	10	8.4	1000	100
2	883	bal	10	8.4	1000	100
3	833	bal	10	8.4	100	100
4	883	bal	10	8.4	100	100
5	833	bal	15	13	100	
6	833	bal	15	13	1000	
7	833	bal	15	13		100
8	833	bal	20	16.8		
9	883	bal	20	16.8		

Table 2. Atmospheres used in the experiments.

mation is produced on corrosion behaviour at temperatures higher than currently in use.

2 Experimental

Test specimens were taken from steel pipes which were originally supplied by Vallourec & Mannessmann Tubes (P91) and Sumimoto (HCM12A). Chemical compositions of the steels are given in Table 1. Specimen size was 0.01 m by 0.01 m by 0.002 m. The final surface finishing of the uncoated specimens was done with 800 grit SiC-paper. For the coating process, the specimens were ground with 320 grit SiC-paper and then cleaned with ethanol in an ultrasonic bath.

Coatings were deposited using a slurry method in which the slurry is brushed on the substrate and when heated, a diffusion coating is produced. The slurry was supplied by Indestructible Paint Ltd. (UK) and it consists of the mixture of xylene isomers and stabilized aluminium powder. According to EDS analyses of a green state coating, small amounts of Si has been used in stabilizing the aluminium powder. Three layers of a slurry were brushed on the specimens, let to dry and then heat treated for 10 hours at 973 K under an argon gas flow. The specimens were cooled to room temperature with the furnace. After the heat treatment, a layer of loose unreacted slurry was left on the specimen surface. It was carefully removed by grinding with a 1200 grit SiC-paper and the specimens were further cleaned in an ultrasonic bath in ethanol, dried and weighed before the tests.

Corrosion tests of 336 hours were carried out in atmospheres containing various amounts of HCl, SO_2, H_2O and O_2 in N_2, the total flow rate being $14.4 \cdot 10^{-3}$ m^3/h. Detailed list of the test atmospheres is given in Table 2. The number of experiments was 9. The used temperatures were 833 K and 883 K. Equilibrium composition of the atmosphere in experiment 1 (Table 2) is shown in the X-Cl-O phase stability diagrams (Figures 1–3). After the tests, the specimens were slowly cooled to room temperature for weighing. Weight gains were used to evaluate the corrosion rate of the specimens.

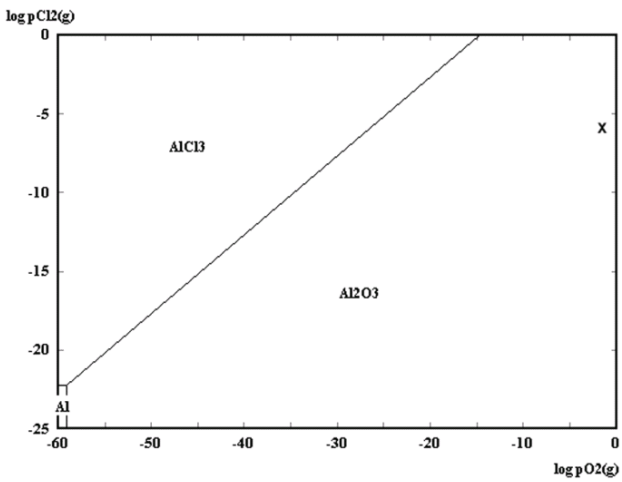

Figure 1. Al-O-Cl phase stability diagram at 833 K. Equilibrium composition of experiment 1 is marked with X.

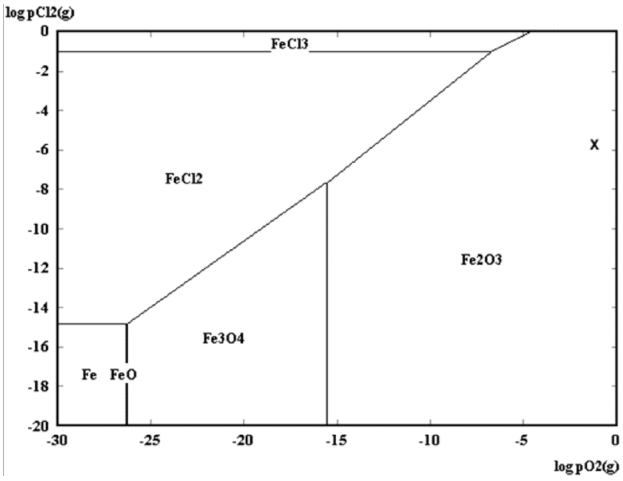

Figure 2. Fe-O-Cl phase stability diagram at 833 K. Equilibrium composition of experiment 1 is marked with X.

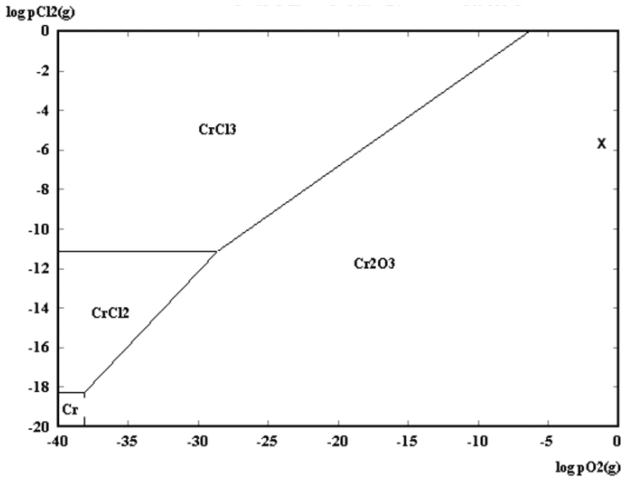

Figure 3. Cr-O-Cl phase stability diagram at 833 K. Equilibrium composition of experiment 1 is marked with X.

Specimen characterization was done by using a Philips XL 30 scanning electron microscope (SEM) equipped with an EDAX energy dispersive spectrometer (EDS) and by employing a Siemens D500 X-ray diffractometer (XRD) and Cu-Kα radiation. In order to study cross-sections, the specimens were sputtered with gold to ensure electrical conductivity, coated electrolytically with nickel and mounted to resin to protect the oxide scales during cutting, grinding and polishing. The nickel coating also provides an excellent contrast between the specimen and the mounting when using back-scattered electrons in SEM investigations.

3 Results and Discussion

3.1 Unexposed Aluminized Specimens

Surface morphology of the aluminized coating was similar on both steels: quite rough (Figure 4 a)), slightly layered (Figure 4 b)) and relatively dense. However, locally on the top of the dense layer, there appeared also a porous surface layer that was only mechanically attached to the dense layer underneath. When studied with EDS, the porous surface layer consisted mainly of aluminium, which suggests that it was primarily sintered slurry. Small cracks were observed on the dense sections of the coating. Most likely, the cracks appeared during cooling because of thermal expansion mismatch between the coating and the substrate [9].

Presence of the Al_5Fe_2, $AlCr_2$ and Cr_3Si phases in the coating was confirmed by XRD (Figure 5). Cross sectional SEM + EDS studies (Figure 6) disclosed distribution of the phases (Figure 7). The $AlCr_2$ and Cr_3Si phases, the latter of which may be detected as brighter of the two in BSE images, appeared as small precipitates in the Al_5Fe_2 phase matrix. A layer of a phase with the composition close to the stoichiometric AlFe was found underneath the Al_5Fe_2phase layer and, finally, the AlN precipitates were detected embedded in the substrate near the coating interface. The findings are supported by previous studies [8, 12].

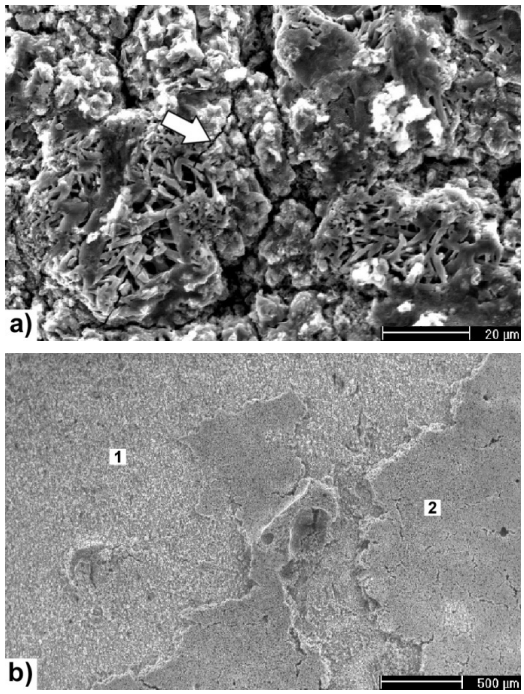

Figure 4. Secondary electron images showing the surfaces of unexposed aluminized specimens. a) P91. A small crack is indicated with an arrow. b) HCM12A. 1) Dense coating layer. 2) Porous surface layer on top of the dense layer.

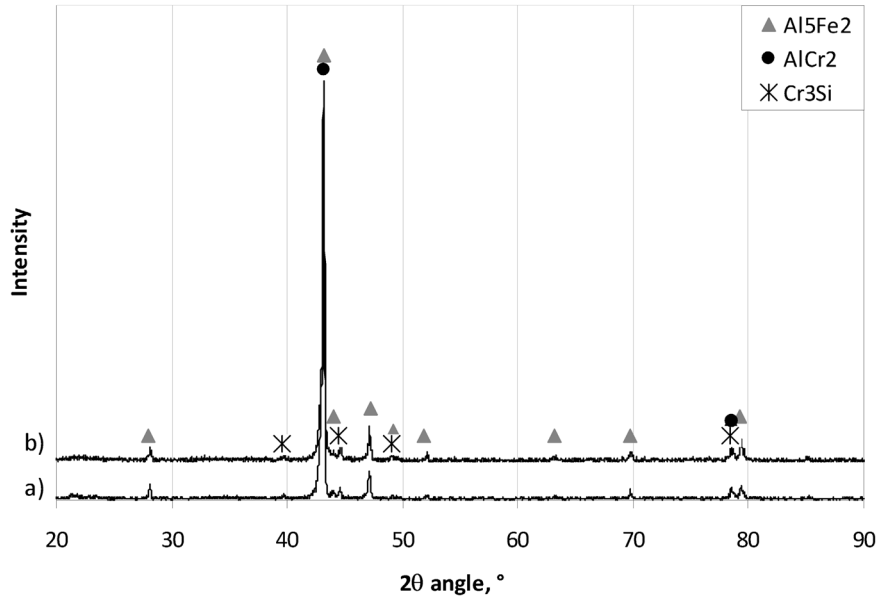

Figure 5. XRD spectra for unexposed aluminized specimens. a) P91. b) HCM12A.

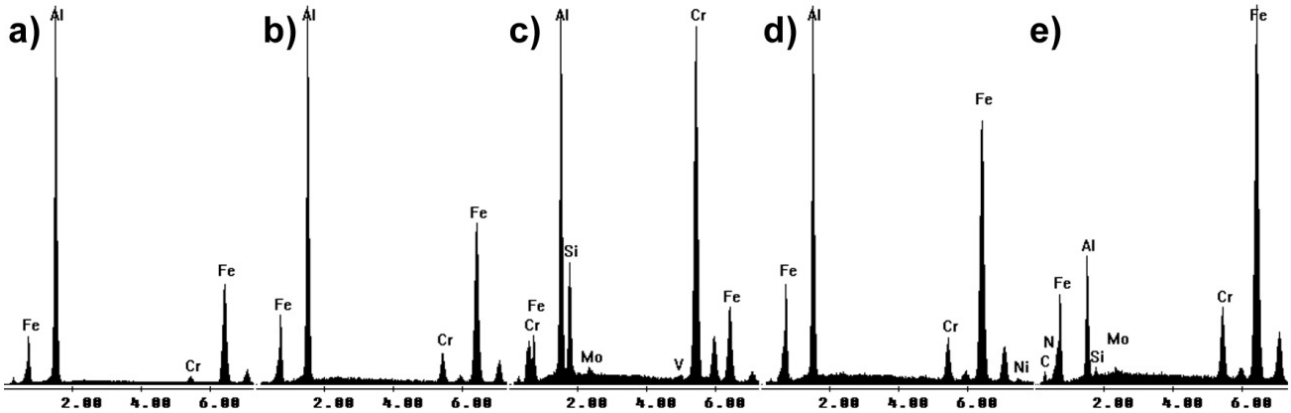

Figure 6. EDS analyses for a cross section of unexposed aluminized P91 (Figure 5 a)). All compositions are given in at-%. a) Al_5Fe_2 (70.6 % Al, 28.2 % Fe, 1.2 % Cr). b) $AlCr_2$ (60.4 % Al, 35.2 % Fe, 4.4 % Cr). c) Cr_3Si (38.3 % Al, 37.6 % Cr, 12.3 % Si, 11.2 % Fe, 0.4 % Mo, 0.3 % V). d) AlFe (50.2 % Al, 44.5 % Fe, 4.5 % Cr, 0.8 % Ni). e) AlN precipitates (65.0 % Fe, 20.7 % Al, 7.9 % Cr, 5.0 % N, 1.0 % Si, 0.3 % Mo).

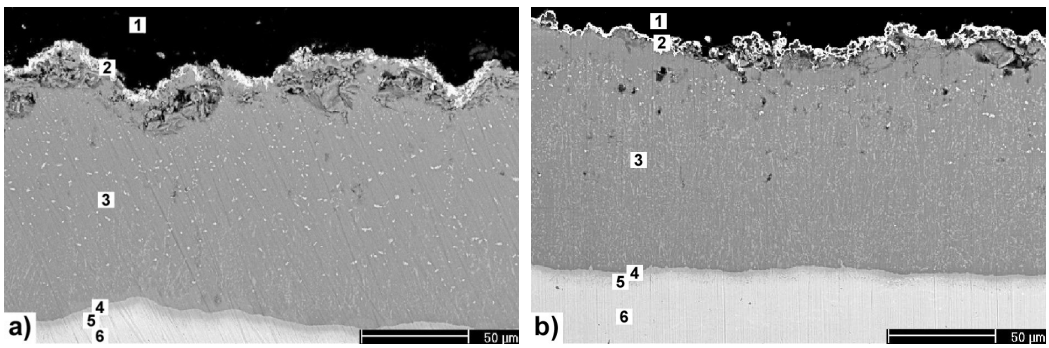

Figure 7. Back scattered electron images showing cross sections of unexposed aluminized specimens. a) P91. b) HCM12A. On both images: 1) Mounting. 2) Nickel coating. 3) Al_5Fe_2 matrix phase (as grey in images) with $AlCr_2$ and Cr_3Si precipitate phases (both as white in images, with the latter shown slightly brighter). 4) AlFe phase. 5) AlN precipitates. 6) Substrate.

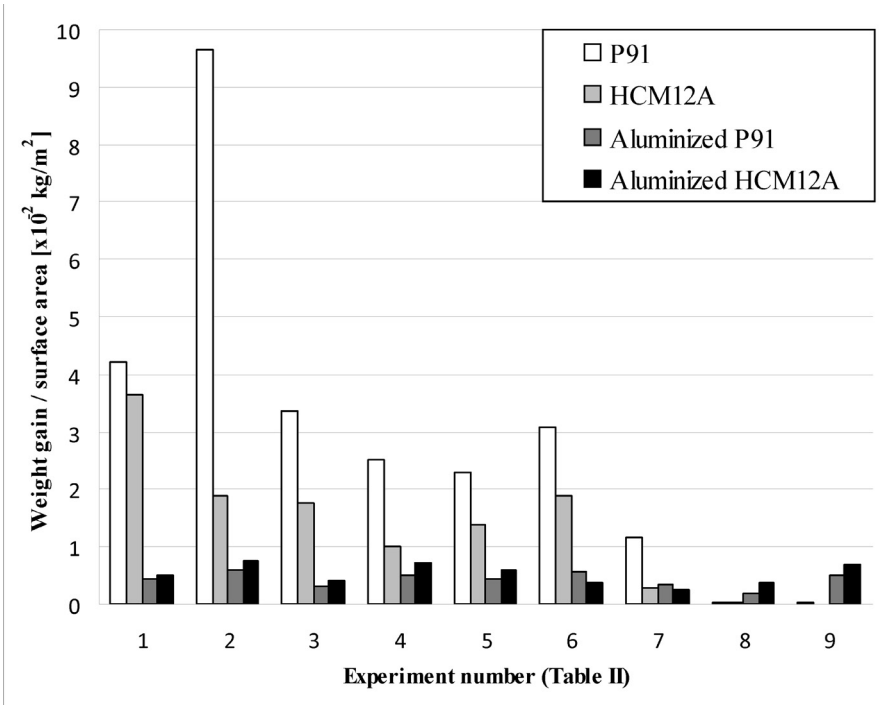

Figure 8. Relative weight gains for specimens exposed for 336 hours. Test atmospheres and temperatures are shown in Table 2.

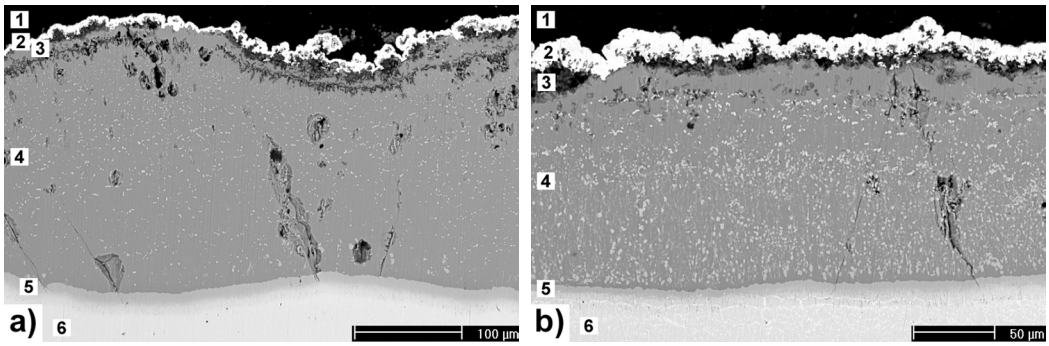

Figure 9. Cross-sections of aluminized specimens after 336 hours at 883 K in $N_2 - 1000$ ppmv $HCl - 100$ ppmv $SO_2 - 10\,\%$ $H_2O - 8.4\,\%$ O_2. a) P91. b) HCM12A. On both images: 1) Mounting. 2) Nickel coating. 3) γ-Al_2O_3. 4) Al_5Fe_2 matrix phase (as grey in images) with $AlCr_2$ and Cr_3Si precipitate phases (both as white in images, with the latter shown slightly brighter). 5) AlFe phase. 6) Substrate.

3.2 Aluminized Specimens After 336 Hour Exposure

Relative weight gains for the specimens after 336 hours exposure to test atmospheres are presented in Figure 8. It can be seen that weight gains for the aluminized specimens were generally much lower than for the uncoated specimens. The aluminized specimens gained systematically more weight at 883 K than at 833 K. Furthermore, composition of the test atmosphere did not have a significant influence on the weight changes for the aluminized specimens. In order to identify the effect of surface roughness, completely ground aluminized specimens were exposed in experiment 6 (Table 2) along the "regular" specimens. Average weight gains for the ground aluminized specimens were $1 \cdot 10^{-3}$ kg/m^2. In comparison, the regular aluminized specimens gained $5 \cdot 10^{-3}$ kg/m^2 in the same experiment.

Cross-sections of the regularly aluminized specimens (Figure 9) reveal that oxidation has taken place on the surface of specimens. This is in line with the phase stability diagram presented in Figure 1, which shows that Al_2O_3 is, by a large margin, the stable phase. XRD-spectra (Figure 10 a) and Figure 10 b)) reveal the presence of some γ-Al_2O_3 along with Al_5Fe_2, $AlCr_2$ and Cr_3Si that comprise the coating. The γ-Al_2O_3 is the typical Al_2O_3 phase that develops on Al-rich surfaces below 1173 K [20]. However, it is suspected that the oxidation reaction occurs mostly be-

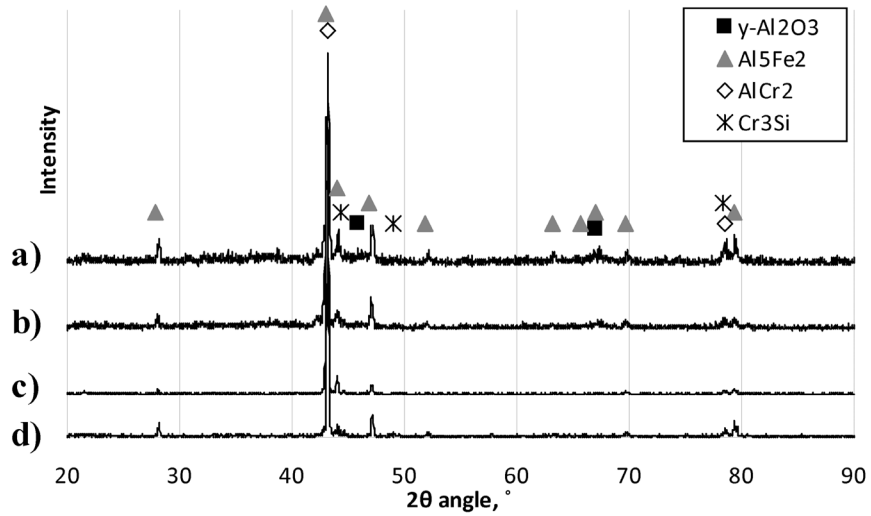

Figure 10. XRD spectra for aluminized specimens after 336 hours exposure under test conditions indicated in brackets (Table 2). a) P91 (2). b) HCM12A (2). c) Completely ground P91 (6). d) Completely ground HCM12A (6).

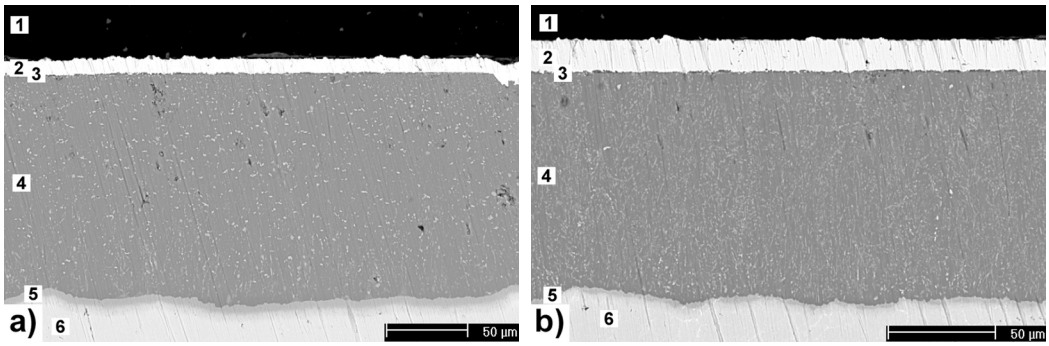

Figure 11. Cross-sections of aluminized, completely ground specimens after 336 hours at 833 K in N_2 − 1000 ppmv HCl − 15 % H_2O − 13 % O_2. a) P91. b) HCM12A. On both images: 1) Mounting. 2) Nickel coating. 3) $\gamma - Al_2O_3$. 4) Al_5Fe_2 matrix phase (as grey in images) with $AlCr_2$ and Cr_3Si precipitate phases (both as white in images, with the latter shown slightly brighter). 5) AlFe phase. 6) Substrate.

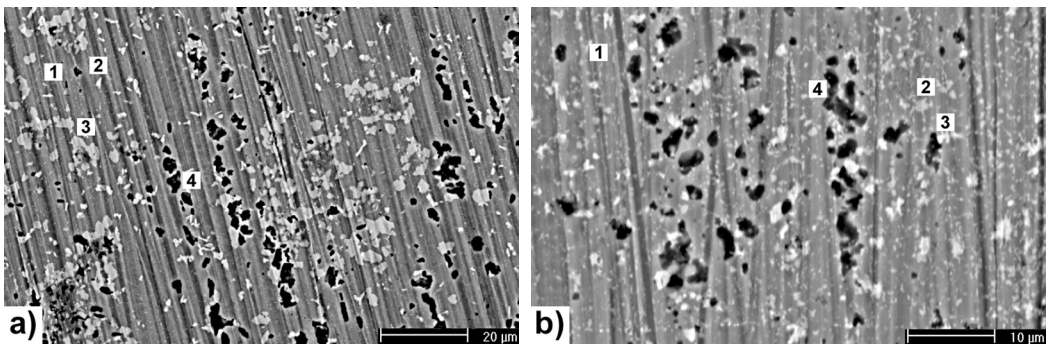

Figure 12. Back scattered electron images showing the surfaces of aluminized, completely ground, specimens after 336 hours at 833 K in N_2 − 1000 ppmv HCl − 15 % H_2O − 13 % O_2. a) P91. b) HCM12A. On both images: 1) Al_5Fe_2 matrix phase (grey). 2) $AlCr_2$ (light grey). 3) Cr_3Si (brighter light grey). 4) Hole (black).

tween the residual unreacted slurry and the atmosphere, because in both Figure 9a and Figure 9b, there are areas with almost no visible corrosion, very similar to the ground aluminized specimens shown in Figure 11. The oxide scales formed on the ground aluminized specimens were very thin and hardly distinguishable in XRD-spectra (Figures 10 c) and Figure 10 d)). BSE-images (Figure 12) of the surfaces of the ground aluminized specimens reveal that some of the $AlCr_2$ and Cr_3Si precipitates have been lost during the test. A possible explanation is that these Cr-rich precipitates have reacted with chlorine in the atmosphere at the scale-metal interface and vaporized off the surface, leaving small holes behind. In the regular specimens, the precipitates were not located directly on the surface and, therefore, not similarly exposed to the atmosphere. However, it is possible that some of the precipitates near the cracks (Figure 9) have also been lost during the tests. Extensive internal grain boundary oxidation, which has been reported for some coated alloys in [14], was not observed in this study.

3.3 Uncoated Specimens After 336 Hour Exposure

Uncoated specimens gained considerably more weight than the aluminized specimens (Figure 8). Of the uncoated specimens, the 12 mass % Cr steel, HCM12A, gained systematically less weight than the 9 mass % Cr steel, P91, in all experiments. The highest weight gains were observed for P91 at 883 K in an atmosphere containing 1000 ppmv HCl and 100 ppmv SO_2 (experiment 2), i.e., under the most severe test conditions. Interestingly, in the same experiment, uncoated HCM12A gained less weight than at 833 K. Similar behaviour, i.e., less corrosion at higher test temperatures, has been previously reported on 12 % Cr steels [13, 21] in water vapour containing environments at temperatures of 873–923 K and is caused by a faster diffusion of Cr to the surface at the higher temperature. However, it has also been reported that after the initial protectivity fails, corrosion rate increases rapidly and, thus, long term predictions should be made with caution.

BSE-image of the cross-section of the uncoated P91 (Figure 13 a), which gained the most weight, shows a layered structure of the corrosion product. A horizontal dividing line can be seen in the middle: it is the original surface of the specimen. According to elemental maps (Figure 13 b)), Cr is enriched in the scale below the original surface, while S is found near the substrate surface. Cl, the key component of active oxidation process, which would also be expected to be found near the substrate, could not be detected at all, probably due to specimen preparation process. The thick layer above the original surface consists of Fe and O, and was identified as Fe_2O_3 by XRD (Figure 14 a)). The uncoated HCM12A (Figure 15) exposed along the uncoated P91 is very similar in structure, but the scale is thinner and has a significantly higher Cr content below the original surface. The elemental maps also disclosed S at the scale-substrate interface. Fe_2O_3 was detected on the scale by XRD (Figure 14 b)). According to the phase stability diagrams shown in Figures 2 and 3, Fe_2O_3 and Cr_2O_3 are the stable phases at 833 K in the atmosphere of experiments 1. They are also stable at 883 K (experiment 2). However, below the scale at the metal-scale interface, pO_2 and pCl_2 are not in the equilibrium state of the atmosphere, which makes *active oxidation* possible. Indeed, the distribution of Cr within the scale supports the view about active oxidation [5].

As expected, lowering the HCl content from 1000 ppmv (experiments 1 and 2) to 100 ppmv (experiments 3 and 4) resulted in smaller weight gains for the uncoated specimens (Figure 5). However, with only 100 ppmv HCl in the atmosphere, the weight gains at 883 K were lower for both of the uncoated materials than at 833 K, which suggests a change in the corrosion process compared to the 1000 ppmv HCl experiment particularly in the case of P91, because of the tenfold increase in S/Cl-ratio. It is known that the presence of large amounts of SO_2 compared to HCl can decrease the corrosion rate, because the presence of SO_2 enhances the stability of formed sulphates and suppresses the chlorine in-

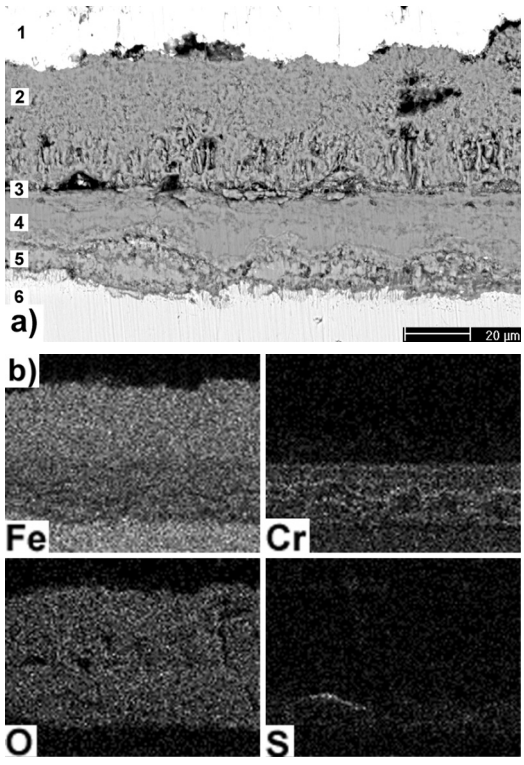

Figure 13. Cross-section of uncoated P91 after 336 hours at 883 K in N_2 − 1000 ppmv HCl − 100 ppmv SO_2 − 10 % H_2O − 8.4 % O_2. a) BSE-image. 1) Nickel coating. 2) Fe_2O_3. 3) Original surface. 4) Cr-rich layer. 5) Layer in which S can be found. 6) Substrate. b) Corresponding elemental maps for Fe, Cr, O and S.

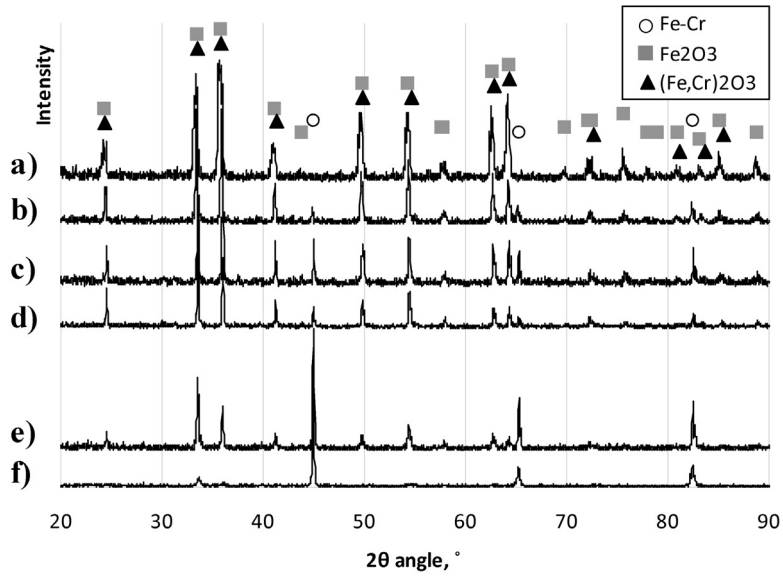

Figure 14. XRD spectra for uncoated specimens after 336 hours exposure in atmosphere indicated in brackets (Table 2). a) P91 (2). b) HCM12A (2). c) P91 (4). d) HCM12A (4). e) P91 (7). f) HCM12A (7).

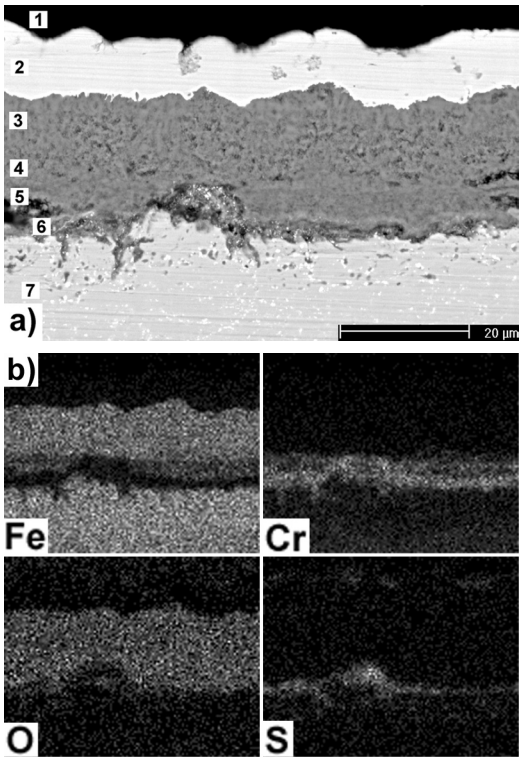

Figure 15. Cross-section of uncoated HCM12A after 336 hours at 883 K in $N_2 - 1000$ ppmv $HCl - 100$ ppmv $SO_2 - 10\,\%$ $H_2O - 8.4\,\%$ O_2. a) BSE-image. 1) Mounting. 2) Nickel coating. 3) Fe_2O_3. 4) Original surface. 5) Cr-rich layer. 6) Cr-rich layer with S. 7) Substrate. b) Corresponding elemental maps for Fe, Cr, O and S.

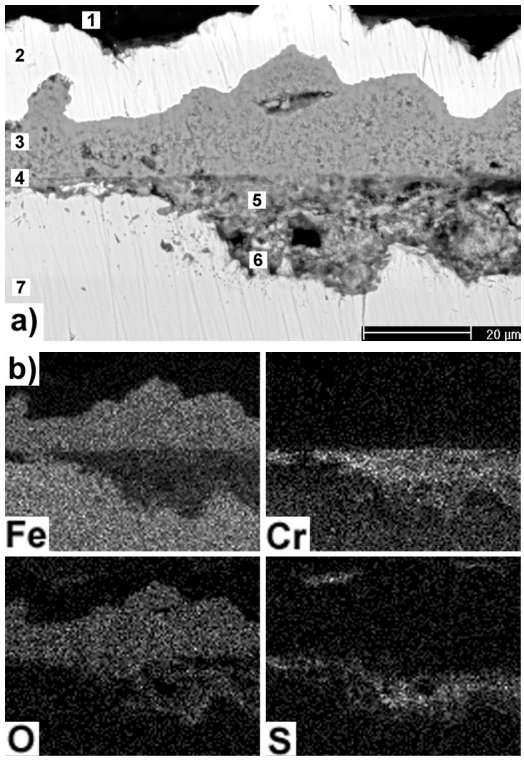

Figure 16. Cross-section of uncoated P91 after 336 hours at 883 K in $N_2 - 100$ ppmv $HCl - 100$ ppmv $SO_2 - 10\,\%$ $H_2O - 8.4\,\%$ O_2. a) BSE-image. 1) Mounting. 2) Nickel coating. 3) Fe_2O_3. 4) Original surface. 5) Cr-rich layer. 6) Layer in which S can be found. 7) Substrate. b) Corresponding elemental maps for Fe, Cr, O and S.

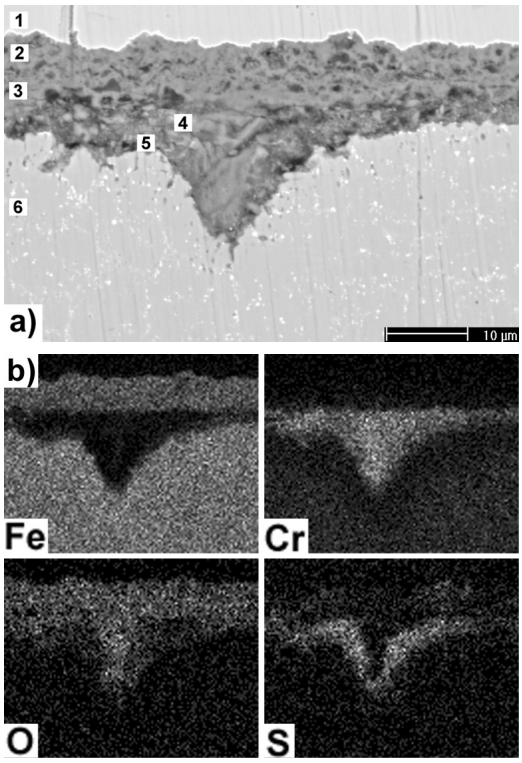

Figure 17. Cross-section of uncoated HCM12A after 336 hours at 883 K in N_2 − 100 ppmv HCl − 100 ppmv SO_2 − 10 % H_2O − 8.4 % O_2. a) BSE-image. 1) Nickel coating. 2) Fe_2O_3. 3) Original surface. 4) Cr-rich layer. 5) Layer in which S can be found. 6) Substrate. b) Corresponding elemental maps for Fe, Cr, O and S.

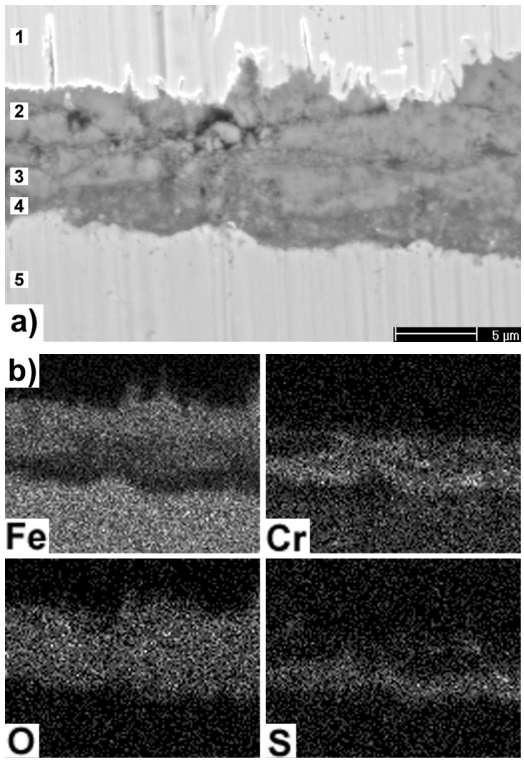

Figure 18. Cross-section of uncoated P91 after 336 hours at 833 K in N_2 − 100 ppmv SO_2 − 15 % H_2O − 13 % O_2. a) BSE-image. 1) Nickel coating. 2) Fe_2O_3. 3) Cr-rich layer. 4) Layer in which S can be found. 5) Substrate. b) Corresponding elemental maps for Fe, Cr, O and S.

duced active oxidation at the metal-scale interface [22]. According to [23], the best way to prevent corrosion in biofuel-firing is to have S/Cl ratio of the fuel above 2, preferably over 4.

Cross-section of the uncoated P91 exposed at 883 K in low HCl and low SO_2 (experiment 4), revealed a varying degree of internal corrosion (Figure 16). The general structure of the scale is very similar to that previously introduced, but, interestingly, there is evidently more Cr and S in the scale than in experiment 2, in which the uncoated P91 had the most severe corrosion. Furthermore, Cr is more evenly distributed within the scale. These observations suggest that vaporization of $CrCl_2$ may have played a smaller role in the corrosion. Cross-section of the corresponding uncoated HCM12A (Figure 17) is similar to the uncoated P91, but there is less internal corrosion and even more Cr present. Furthermore, here S forms almost a continuous layer. Fe_2O_3 is detected by XRD (Figures 14 c) and Figure 14 d)), and also Cr_2O_3 may exist in the Cr-rich layer below the original surface level (many of the XRD peaks of Fe_2O_3 and Cr_2O_3 overlap or are very close to each other).

It was observed that, at 833 K without the presence of SO_2 in the atmosphere, the increase of HCl concentration from 100 ppmv to 1000 ppmv (experiments 5 and 6) introduced greater weight gains for both of the uncoated materials. However, the weight gains were smaller as compared to experiments 1 and 3 with combined effect of HCl and SO_2, indicating that the presence of SO_2 in the atmosphere accelerated the corrosion. On the other hand, it should be noted that the amounts of O_2 and H_2O in experiments 5–7 were slightly different from those in experiments 1–4. Changing the H_2O content has been shown [18] to influence weight gains in a parallel experiment, but a clear trend was not identified. Exposure to SO_2 containing atmosphere without HCl (experiment 7) resulted in lower weight gains for the uncoated specimens than exposure in any of the HCl containing atmospheres. Again, P91 gained more weight than HCM12A, the weight gains of the latter being of the same order than those for the aluminized specimens.

Cross-section of the uncoated P91 exposed in experiment 7 (Figure 18 a)) shows a thin scale without a clear layered structure, which was observed in the connection of combined HCl + SO_2 atmosphere. However, the corresponding elemental maps (Figure 18 b)) combined with XRD spectra (Figure 14 e)) suggest similar composition of the scale to the previous cross-sections. Cross-section of the uncoated HCM12A (Figure 19 a)) exposed along the un-

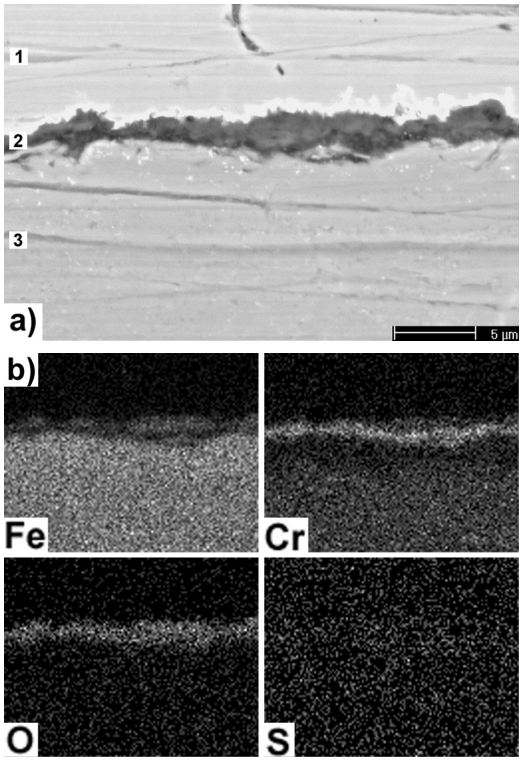

Figure 19. Cross-section of uncoated HCM12A after 336 hours at 833 K in N_2-100ppmv $SO_2-15\,\%H_2O-13\,\%O_2$. a) BSE-image. 1) Nickel coating. 2) Cr-rich layer. 3) Substrate. b) Corresponding elemental maps for Fe, Cr, O and S.

coated P91 shows even a thinner scale. The corresponding elemental maps (Figure 19 b)) reveal that the scale is mostly enriched in Cr with some Fe on top. Based on XRD-spectra (Figure 14 f)), existence of Fe_2O_3 and Cr_2O_3 is suggested. S was not detected in significant amounts in the scale, indicating that the scale protects the substrate.

Experiments in air-water vapour resulted in very little overall corrosion, but there were some areas (Figure 20) where formation of a thicker oxide scale had begun, thus indicating that with a longer exposure time, *break away*, could initiate [24]. Therefore, making long term predictions based on a short exposure time should be avoided.

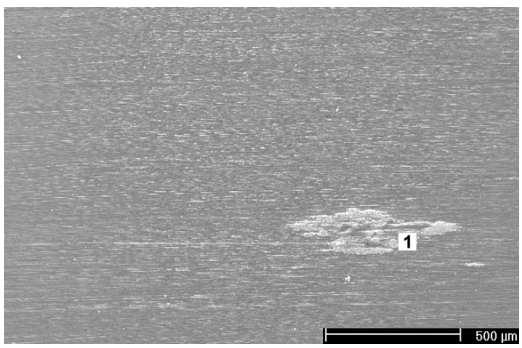

Figure 20. Secondary electron image showing the surface of uncoated P91 after 336 hours at 883 K in $N_2 - 20\,\%H_2O - 16.8\,\%O_2$. 1) Thicker scale.

4 Conclusions

Two 9–12 % Cr steels, P91 and HCM12A, were coated with an aluminium diffusion coating and exposed along uncoated steels to a series of 336 hour experiments in atmospheres containing varying amounts of O_2, H_2O, HCl and SO_2 at 833 and 883 K. It was observed that application of aluminized coatings resulted in a clear improvement in corrosion resistance of the steels. Weight gains for the aluminized specimens were influenced primarily by temperature used in the experiments, not by the test atmospheres. The increases in weight at the higher temperature were not significant and the aluminium diffusion coating remained dense and protective. Thin γ-Al_2O_3 scales were identified on their surface.

The uncoated specimens gained significantly more weight than the aluminized specimens in most of the experiments. As expected on the basis of their Cr contents, P91 (9 % Cr) gained systematically more weight than HCM12A (12 % Cr) in the experiments. Overall, the formed corrosion scale had a similar structure on both steels: an external layer of Fe_2O_3 and an Cr-containing oxidized layer below the original surface level. S was found at the scale-metal-interface in most SO_2 containing atmospheres. However, Cl was not found, even though the amount of HCl in the atmosphere had a clear influence on weight gains. It is therefore assumed that Cl was present at the scale-metal interface and active oxidation took place, but Cl was probably lost due to specimen preparation process. Distribution of Cr in the scales formed in HCl-containing atmospheres further supports active oxidation.

Acknowledgments

The authors would like to thank the Academy of Finland (decisions 111948, 106160 and 218296) for financial support.

References

[1] T. R. Miles, T. R. Miles Jr., L. L. Baxter, R. W. Bryers, B. M. Jenkins and L. L. Oden, *Biomass Bioenergy*, **10** (1996), 125–138.

[2] B. Sander, *Biomass Bioenergy*, **12** (1997), 177–183.

[3] L. L. Baxter, T. R. Miles, T. R. Miles Jr., B. M. Jenkins, D. Dayton, T. Milne, R. W. Bryers and L. L. Oden, *Fuel Process. Technol.*, **54** (1998), 47–78.

[4] N. Otsuka, *Corros. Sci.*, **44** (2002), 265–283.

[5] F. H. Stott and C. Y. Shih, *Oxid. Met*., **54** (2000), 425–443.

[6] A. Zahs, M. Spiegel and H. J. Grabke, *Corros. Sci.*, **42** (2000), 1093–1122.

[7] H. P. Nielsen, F. J. Frandsen, K. Dam-Johansen and L. L. Baxter, *Prog. Energy Combust. Sci.*, **26** (2000), 283–298.

[8] A. Agüero, R. Muelas, M. Gutiérrez, R. Van Vulpen, S. Osgerby and J. P. Banks, *Surf. Coat. Technol.,* **201** (2007), 6253–6260.

[9] A. Agüero, R. Muelas, A. Pastor and S. Osgerby, *Surf. Coat. Technol.*, **200** (2005), 1219–1224.

[10] F. J. Pérez and S. I. Castañeda, *Surf. Coat. Technol.*, **201** (2007), 6239–6246.

[11] V. Rohr, A. Donchev, M. Schütze, A. Milewska and F. J. Pérez, *Corros. Eng. Sci. Technol*., **40** (2005), 226–232.

[12] E. Huttunen–Saarivirta, F. H. Stott, V. Rohr and M. Schütze, *Corros. Sci.*, **49** (2007), 2844–2865.

[13] J. Metsäjoki, E. Huttunen-Saarivirta and T. Lepistö, J. *J. Mater. Eng. Perform.*, 20 (2011), 298–305.

[14] J. Kalivodova, D. Baxter, M. Schütze and V. Rohr, *Mater. Corros.*, **56** (2005), 882–889.

[15] J. Kalivodova, D. Baxter, M. Schütze and V. Rohr, *Mater. Corros.*, **59** (2008), 367–373.

[16] H. J. Grabke, M. Spiegel and A. Zahs, *Mat. Res.*, **7** (2004), 89–95.

[17] Y. Kawahara, *Mater. Corros.*, **57** (2006), 60–72.

[18] M. Sánchez Pastén and M. Spiegel, *Mater. Corros.*, **57** (2006), 192–195.

[19] A. Agüero, M. Gutiérrez and V. González, *Mater. High Temp.*, **25** (2008), 257–265.

[20] P. Kofstad, *High Temperature Corrosion*, Elsevier applied Science Publishers ltd., Essex, England (1988).

[21] J. Zurek, E. Wessel, L. Niewolak, F. Schmitz, T.-U. Kern, L. Singheiser and W. J. Quadakkers, *Corros. Sci.*, **46** (2004), 2301–2317.

[22] H. J. Grabke, E. Reese and M. Spiegel, *Corros. Sci.*, **37** (1995), 1023–1043.

[23] O. H. Larsen and N. Henriksen, *in: Power Plant Chemical Technology* 1996, Kolding, Denmark, 4–6 September 1996, Elsam, pp. 7.1–7.18

[24] D. A. Jones, *Principles and Prevention of Corrosion*, Macmillan Publishing Company, USA (1992).